Journal of Quality Measurement and Analysis *JQMA* 19(3) 2023, 41-53
e-ISSN: 2600-8602 *http://www.ukm.my/jqma*

CARREAU HYBRID NANOFILM FLOW OVER A STRETCHING SHEET WITH SUCTION/INJECTION EFFECT

(*Aliran Nanofilem Carreau Hibrid di Atas Lembaran Regangan dengan Kesan Sedutan/Suntikan*)

DIAN ADLINE JALALUDDIN*, ROSLINDA NAZAR, KOHILAVANI NAGANTHRAN & ISHAK HASHIM

ABSTRACT

The current work investigates the thin liquid film flow problem in the Carreau hybrid nanofilm (Al_2O_3-Cu/H_2O) on a stretching sheet numerically. There is a suction/injection effect at the stretching sheet's surface, which is permeable. The boundary value problem solver (bvp4c) in MATLAB is applied to solve the system of linear equations obtained from the partial differential equations by employing suitable similarity variables. The effect of suction was found to contribute to improving heat transfer performance. The suction parameters had a more significant impact on the skin friction coefficient and heat transfer rate than the injection parameters. It was determined that the diminution of the film thickness at the free surface and the improvement of convective heat transfer rates were the most significant effects of the injection.

Keywords: thin film flow; hybrid nanofilm; Carreau fluid

ABSTRAK

Kajian ini mengkaji tentang masalah aliran filem cecair nipis dalam nanofilem nipis Carreau (Al_2O_3-Cu/H_2O) pada helaian regangan secara berangka. Terdapat kesan sedutan/suntikan pada permukaan helaian regangan yang telap. Penyelesaian masalah nilai sempadan (bvp4c) dalam MATLAB digunakan untuk menyelesaikan sistem persamaan linear yang diperoleh daripada persamaan pembezaan separa dengan menggunakan pembolehubah persamaan yang sesuai. Kesan sedutan didapati menyebabkan peningkatan prestasi pemindahan haba yang lebih baik. Parameter sedutan mempunyai kesan yang lebih ketara ke atas pekali geseran kulit dan kadar pemindahan haba daripada parameter suntikan. Didapati juga bahawa pengurangan ketebalan filem pada permukaan bebas dan peningkatan kadar pemindahan haba perolakan terhadap kesan suntikan adalah yang paling ketara.

Kata kunci: aliran filem nipis; nanofilem hibrid; cecair Carreau

1. Introduction

The thin liquid film is an emerging technology in the manufacturing industry with promising applications such as polymer processing, reactor fluidisation, and wire/fiber coating. A smooth surface is necessary for the coating process to provide the best product appearance and achieve qualities like minimal friction, transparency, and strength (Dandapat *et al*. 2003). Furthermore, for most industrial purposes, such as batteries, thin-film solar cells, and photovoltaic cells, thin-film flow is a necessity (Iqbal *et al*. 2020). As a protective coating applied to the extrudate, Wang (2006) dealt with the problem of the thin liquid film flow across an unsteady stretched sheet that simulates new paint. Andersson *et al*. (2000) enhanced the findings of Wang (1990) by introducing a new similarity transformation and incorporating the characteristics of heat transfer for the dimensionless temperature. Since the heat transfer and flow within a thin liquid film above the stretched surface dramatically impacts the quality of the finished products in

many manufacturing industries, Liu (2004) highlighted the significance of conducting thorough analysis and building a basic knowledge of momentum and heat transfers in such systems. Several works in literature, for example, see Alabdulhadi *et al*. (2023) examines the heat transfer and unsteady thin film flow of Al_2O_3 water nanofluid over an inclined stretching sheet that exhibits the impact of buoyancy force. The findings indicate that decreasing the film thickness occurs when the unsteadiness and magnetic parameters are increased. Moreover, In order to study the unstable thin film flow dynamic and heat transmission, Ali *et al*. (2022) used Al_2O_3 nanofluid through a stretched sheet with convective boundary conditions.

Since nanofluid boundary layer flow has essential applications in contemporary technology, several researchers have dedicated their work to this field. Nanofluids have risen thermal conductivity, resulting in a higher nanoparticle volume. For instance, Tham *et al*. (2012) investigated the steady mixed convection boundary layer flow adjacent to the lower stagnation point of a horizontally oriented circular cylinder with a constant surface temperature, which is placed within a porous medium saturated by a nanofluid containing gyrotactic microorganisms. The thermal conductivity of the nanoliquid layer across an unsteady stretched surface was modeled by Narayana and Sibanda (2012) using a practical medium theory-based approach, and Xu *et al*. (2013) discovered that adding nanoparticles to base fluids may significantly enhance heat transfer properties. On the contrary, a hybrid nanofluid is a fluid that has been deliberately created and is made up of a homogenous combination of more than two nanoparticles with novel chemicals and physical properties. For instance, the coolant in welding and machining benefits from the hybrid nanofluid capability to provide the necessary heat transfer impact at minimal particle concentration. The innovative concept of the metal component being suspended in the liquid at a nanoscale to elevate the rate of heat transfer was introduced by Choi and Eastman (1995). The hybrid nanofluid is suggested to address this problem in research studies by Suresh *et al*. (2011) and Sundar *et al*. (2014). Moreover, the hybrid nanofluid was able to attract the curiosity of many scientists; see (Minea 2017; Waini *et al*. 2020; Zainal *et al*. 2020a; 2020b; Waini *et al*. 2021).

Carreau was the one who initially proposed the general Newtonian Carreau liquid (Carreau 1972). The model comes out to be reasonably suited via the disruptions in polymer performance at various stream places. In general, meltdown and some outcomes from diluted polymers are well matched by the Carreau model. Furthermore, it defines the shear thickening and shear thinning that characterise the behavior of many non-Newtonian liquids. Several researchers went on to discover the Carreau liquid model and its implementation in various natural and later scientific breakthroughs. Myers (2005) concluded that the Carreau liquid model is the preferred choice for thin film flow due to its high level of precision, considering the potential of the generalized non-Newtonian fluid. As a result, numerous important research papers have been released regarding the flow of Carreau thin film; see (Tshehla 2011; Khan *et al*. 2019; Naganthran *et al*. 2020a). The dual solutions of the Carreau liquid stagnation point stream in the vicinity of a porous stretched surface were discovered by Akbar *et al*. (2014). Moreover, numerous geometries were used by Abbasi *et al*. (2015) and Khan *et al*. (2019) to investigate the thermodynamics of a Carreau fluid thin film. The Carreau liquid thin layer plus energy transfer through a porous expanding surface was determined by Naganthran *et al*. (2020b). Researchers have reported several studies on the Carreau thin liquid film flow. Bilal *et al*. (2021), for instance, increased the mass and energy transfer rate across a stretching surface by examining the Carreau fluid of the thin film flow while incorporating Marangoni convection, a uniform magnetic field, and couple stress. Naganthran *et al*. (2021) investigated the melting heat transfer impact on the thin film flow of the Carreau hybrid nanofluid across a stretched

sheet. They found that the transport phenomenon behavior connected to negative film thickness was an unreliable method.

Thus, the injection or suction phenomena are crucial to gain an improved understanding of the boundary layer flow. By inducing suction at the surface of the moving body, thus the boundary layer thickness is adjusted. Mukhopadhyay (2013) asserts that injection or suction of fluid through the boundary layer may drastically alter the flow field. As with the design of thermal oil recovery, thrust bearings, and radial diffusers, the suction and blowing processes are vital in many engineering operations. Suction generally contributes significantly to increasing skin friction, while injection has the reverse effect. In the polymer industry, several implementations, such as polymer fiber coating, wires, and film cooling, involve boundary layer control applications; thus, fluid injection over a porous bounding wall is frequently attention in these practical situations. In a chemical reaction, the reactants are added by injection and removed by suction, respectively. It lowers the drag by cooling the surface and prevents corrosion or scaling.

The present work aims to employ the model in Wang (2006) and consider the suction/injection effects in the Carreau hybrid thin film across a stretching surface. Hence, the present formulation of the problem has reduced the nonlinear differential equation into ordinary differential equations that can be solved by employing Wang (2006) similarity transformation. The current study is significant in the coating process because it overcomes the shortcomings of the previous mathematical model for thin Careau hybrid nanofluid flow over a stretched sheet. As a result, the theoretical study advances our knowledge and improvement of coating processes, which are critical in many industrial applications such as medicinal appliances, electronics, and optics. Furthermore, by applying the built-in collocation method, the bvp4c in MATLAB, the formulated mathematical model has been resolved to yield approximate solutions. Up until now, the method mentioned above has been utilized to solve fewer problems related to thin film flow, particularly for thin Careau hybrid nanofilm flow. This study was effective in identifying the effects of the various values of nanoparticles, the unsteadiness parameter, the power-law index, the Prandtl number, and the influences of the suction/injection parameter on the numerical results are discussed in detail. Subsequently, this work is strongly acknowledged to be new and original.

2. Problem Formulation

The flow of the Carreau fluid was regarded as unsteady and incompressible in two-dimensional, with a constant thickness, $h(t)$ for the thin liquid film. The origin of the Cartesian coordinate system defines the boundary of the Carreau fluid flow, which is enclosed by a thin liquid film and an accelerating sheet in a horizontal position. The flow setting is depicted in Figure 1, and the $x-$coordinate is oriented perpendicular to the $y-$coordinate. The fluid motion bounded by the thin film and the sheet accelerated is caused by the accelerating surface action, representing the stretched sheet position. The stretching sheet with the velocity is given by

$$u_w(x,t) = \frac{bx}{(1-dt)}, \tag{1}$$

where b and k are positive constants with dimension time^{-1}, $dt \neq 1$, while $b > 0$ initial the stretching rate. The surface of the sheet is molten and impermeable. The fluid temperature is signified by T, and the wall temperature, T_w is described as (Tlili *et al*. 2021)

$$T_w = T_s - T_0\sqrt{\frac{b^2x^4}{4v_f^2(1-kt)}}, \quad \text{and} \quad 0 \le T_0 \le T_s. \tag{2}$$

The reference temperature and slit temperature are indicated by T_0 and T_s, respectively. In addition, the end impacts and gravity are believed to be negligible and are thus excluded. The validity of the boundary layer model proposed in the present study is limited to situations where the thickness of the liquid film and the thickness of the boundary layer do not overlap. However, the current model formulation is rendered unreasonable (Maity *et al*. 2016). The smooth and waveless surface is also attributed to the thin planar liquid layer (Andersson *et al*. 2000).

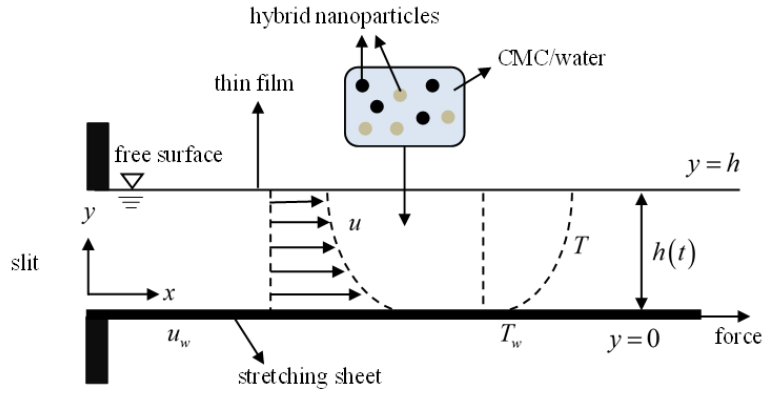

Figure 1: The thin film flow of a physical diagram across a stretched surface

The Carreau fluid's Cauchy stress tensor is written as (Myers 2005)

$$\tau = -pI + \eta A_1, \tag{3}$$

where

$$\eta = \eta_\infty + (\eta_0 - \eta_\infty)[1 + (\lambda\dot{\gamma})^2]^{\frac{n-1}{2}}. \tag{4}$$

Wherein, η is the apparent viscosity, η_∞ denotes the infinite–shear–rate viscosity, η_0 signifies the zero-shear-rate viscosity, I implies the identity tensor, τ is the Cauchy stress tensor, p represents the pressure, n denotes the power-law index, and λ is the material time constant. The shear rate, $\dot{\gamma}$ can be defined as

$$\dot{\gamma} = \sqrt{\frac{1}{2}(\dot{\gamma}:\dot{\gamma})} = \sqrt{\frac{1}{2}\Pi} = \sqrt{\frac{1}{2}tr(A_1^2)} = \sqrt{\frac{1}{2}\sum_i\sum_j \dot{\gamma}_{ij}\dot{\gamma}_{ji}}, \tag{5}$$

where

$$A_1 = (grad\, V) + (grad\, V)^T \tag{6}$$

while A_1 is the Rivlin–Ericksen tensor stated more in Eq. (6) and Π represents the second invariant strain rate tensor in Eq. (5).

Contemplate the situations when $\eta_0 \gg \eta_\infty$ is most applicable. Typically, the extrapolation process determines the η_∞ value or is fixed to zero (recommended theoretical value) (Boger 1977). As a result, the η_∞ value is amended to zero in the current work, which causes Eq. (3) to change to

$$\tau = -pI + \eta_0[1 + (\lambda\dot{\gamma})^2]^{\frac{n-1}{2}} A_1. \tag{7}$$

In the model of Carreau fluid, the characteristics of the Newtonian lies at $(n = 0)$, dilatant lies at $(n > 1)$, and pseudoplastic lies within $(0 < n < 1)$, exhibited where n is the power-law index. Thus, the Carreau fluid governing liquid film flow can be defined as

$$\frac{\partial u}{\partial x} + \frac{\partial v}{\partial y} = 0, \tag{8}$$

$$\frac{\partial u}{\partial t} + u\frac{\partial u}{\partial x} + v\frac{\partial u}{\partial y} = \frac{\mu_{hnf}}{\rho_{hnf}}\frac{\partial^2 u}{\partial y^2}\left[1 + \lambda^2\left(\frac{\partial u}{\partial y}\right)^2\right]^{\frac{n-1}{2}} + \frac{\mu_{hnf}}{\rho_{hnf}}(n-1)\lambda^2\frac{\partial^2 u}{\partial y^2}\left(\frac{\partial u}{\partial y}\right)^2\left[1 + \lambda^2\left(\frac{\partial u}{\partial y}\right)^2\right]^{\frac{n-3}{2}}, \tag{9}$$

$$\frac{\partial T}{\partial t} + u\frac{\partial T}{\partial x} + v\frac{\partial T}{\partial y} = \frac{k_{hnf}}{(\rho C_p)_{hnf}}\frac{\partial^2 T}{\partial y^2}, \tag{10}$$

where u is the velocity components along the $x-$directions and v are the velocity components along the $y-$directions. Meanwhile, $(\rho C_p)_{hnf}$ represents the heat capacity, ρ_{hnf} is density, k_{hnf} implies thermal conductivity, and μ_{hnf} is the hybrid nanofluid dynamic viscosity. The details of $(\rho C_p)_{hnf}$, k_{hnf}, ρ_{hnf}, and μ_{hnf} are shown in Table 1.

Table 1: Definitions of the correlation coefficients of the hybrid nanofluid (Takabi & Salehi 2014)

Properties	Al_2O_3-Cu/(CMC/H_2O) mathematical relation
Density	$\rho_{hnf} = (1-\phi_{hnf})\rho_f + \phi_1\rho_{s1} + \phi_2\rho_{s2}$
Thermal capacity	$(\rho C_p)_{hnf} = (1-\phi_{hnf})(\rho C_p)_f + \phi_1(\rho C_p)_{s1} + \phi_2(\rho C_p)_{s2}$
Dynamic viscosity (Brinkman model)	$\mu_{hnf} = \frac{\mu_f}{(1-\phi_{hnf})^{2.5}}$
Electrical conductivity	$\frac{\sigma_{hnf}}{\sigma_f} = \left[\frac{\left(\frac{\phi_1\sigma_{s1}+\phi_2\sigma_{s2}}{\phi_{hnf}}\right) + 2\sigma_f + 2(\phi_1 k_{s1} + \phi_2 k_{s2}) - 2\phi_{hnf}k_f}{\left(\frac{\phi_1\sigma_{s1}+\phi_2\sigma_{s2}}{\phi_{hnf}}\right) + 2\sigma_f - (\phi_1\sigma_{s1} + \phi_2\sigma_{s2}) + \phi_{hnf}\sigma_f}\right]$
Thermal conductivity (Maxwell model)	$\frac{k_{hnf}}{k_f} = \left[\frac{\left(\frac{\phi_1 k_{s1}+\phi_2 k_{s2}}{\phi_{hnf}}\right) + 2k_f + 2(\phi_1 k_{s1} + \phi_2 k_{s2}) - 2\phi_{hnf}k_f}{\left(\frac{\phi_1 k_{s1}+\phi_2 k_{s2}}{\phi_{hnf}}\right) + 2k_f - (\phi_1 k_{s1} + \phi_2 k_{s2}) + \phi_{hnf}k_f}\right]$

Table 1 indicates that $\phi = 0$ diminishes the model into a normal fluid and the nanoparticle volume percentage is ϕ. Moreover, ϕ_1 signifies the (Al_2O_3) nanoparticle volume fraction and ϕ_2 is Cu nanoparticle volume fraction. In addition, the total volume concentration is given by

$$\phi_{hnf} = \phi_1 + \phi_2 \tag{11}$$

where the two distinct types of nanoparticles suspended in the hybrid nanofluid.

Consequently, ρ_f, k_f and $(\rho C_p)_f$ is the densities, thermal conductivities, and heat capacitance of the base fluid, respectively. Based on physical presumptions, these correlations reinforce the mass and energy-conservation principle. Table 2 presents the physical parameters of the Alumina (Al_2O_3) nanofluids, copper (Cu) nanofluids, and base fluid (sodium carboxymethyl cellulose (CMC)/water).

Table 2: The thermophysical properties of base fluid (sodium carboxymethyl cellulose (CMC)/water) and selected nanoparticles (Oztop & Abu-Nada 2008; Abo-Elkhair *et al*. 2021)

Properties	C_p(J/kgK)	ρ(kg/m^3)	$k\left(\frac{W}{\mathrm{mK}}\right)$	$\hat{\beta} \times 10^{-5}$(mK)
Al_2O_3	765	3970	40	0.85
Cu	385	8933	400	1.67
CMC/H_2O (0-0.3%)	4179	997.1	0.613	21

Eqs. (8)-(10) are coherent with the boundary conditions as follows:

$$\begin{aligned} &t<0:\ u=0,\quad v=0,\quad T=\frac{\partial T}{\partial y}=0 \text{ for all } x \text{ and } y.\\ &t\geq 0:\ u=U_w(x,t),\quad v=v_w,\quad T=T_w \quad \text{at} \quad y=0,\\ &\qquad \mu_{hnf}\frac{\partial u}{\partial y}=0,\quad \frac{\partial T}{\partial y}=0,\quad v=\frac{dh}{dt} \quad \text{at} \quad y=h. \end{aligned} \tag{12}$$

The fluid motion through $v = dh/dt$ is subjected to the kinematic restriction at $y = h$. As a result, at the adiabatic free surface, the heat flux and the wall shear stress completely vanish and thus $\partial u/\partial y = \partial T/\partial y = 0$ at $y = h$. Consequently, the following similarity transformations are given (Andersson *et al*. 2000):

$$\begin{aligned} &\psi=\beta x\sqrt{\frac{\nu_f b}{1-dt}}f(\eta),\quad u=\frac{\partial\psi}{\partial y}=\frac{bx}{1-dt}f'(\eta),\quad v=-\frac{\partial\psi}{\partial x}=-\beta\sqrt{\frac{\nu_f b}{1-dt}}f(\eta),\\ &\theta(\eta)=\frac{T-T_w}{T_0-T_w},\qquad T=T_s-T_0\left(\frac{bx^2}{2\nu_f}\right)\frac{1}{\sqrt{(1-dt)^3}}\theta(\eta), \end{aligned} \tag{13}$$

$$\eta=\frac{y}{\beta}\sqrt{\frac{b}{\nu_f(1-dt)}}, \tag{14}$$

where prime deduces the derivative with respect to η. The continuity equation is solved by applying the similarity conversion as in Eq. (13) and Eq. (14) to the governing model Eqs. (9)-(12), and the remaining equations are then transformed as follows:

$$\left(\frac{\mu_{hnf}/\mu_f}{\rho_{hnf}/\rho_f}\right)\left(1+\frac{nWe^2}{R}f''^2\right)\left(1+\frac{We^2}{R}f''^2\right)^{\frac{n-3}{2}}f'''+R\left(ff''-\frac{\sigma\eta}{2}f''-f'^2-\sigma f'\right)=0, \tag{15}$$

$$\frac{k_{hnf}/k_f}{\left(\rho C_p\right)_{hnf}/\left(\rho C_p\right)_f}\theta'' + \Pr R\left(f\theta' - 2f'\theta - \frac{\eta\sigma}{2}\theta' - \frac{3\sigma}{2}\theta \right) = 0, \tag{16}$$

together with the boundary conditions:

$$f(0) = S, \quad f'(0) = 1, \quad f(1) = \sigma/2, \quad f''(1) = 0, \quad \theta(0) = 1, \quad \theta'(1) = 0, \tag{17}$$

while presenting the constant mass transfer parameter, $S = -\frac{v_w}{\beta}\sqrt{\frac{1-dt}{\nu_f b}}$, with a setup where the suction effect appears with $S > 0$, while the injection situation occurs with $S < 0$, the local Weissenberg number is formulated as $We = \sqrt{\frac{\lambda^2 b^3 x^2}{\nu_f (1-dt)^3}}$, the Prandtl number is defined as $\Pr = \frac{\left(C_p\right)_f \mu_f}{k_f}$, and $\sigma = \frac{d}{b}$ signifies the dimensionless measure of unsteadiness. It is highlighted here that setting $n = 1$ and $We = 0$ affect the model in Eqs. (14)-(17) to exhibit the Newtonian characteristics. Thus, the solution of Eq. (15) subject to the boundary conditions in Eq. (17) for fixed value of δ would be locally similar. The dimensionless quantity δ is determined at any $x-$ station according to the local similarity approach, and the influence of the upstream flow history on the similarity variable is disregarded, except in cases where it has an impact (Rahman 2011).

Meanwhile, $R = \beta^2$ is an unknown constant that has to be determined during the process of solving the problem. Next, β is an unknown constant that depicts the dimensionless film thickness and indicates the value of similarity variable (η) at the free surface; hence the expression in Eq. (14) may be written as,

$$\beta = h\sqrt{\frac{b}{\nu_f (1-dt)}}. \tag{18}$$

This unknown constant β must be calculated as integral to the boundary-value problem. Thus,

$$\frac{dh}{dt} = -\frac{d\beta}{2}\sqrt{\frac{\nu_f}{b(1-dt)}}, \tag{19}$$

explicates the change in the film thickness rate. However, the Eq. (15) and Eq. (16) of Carreau fluid model disclose Newtonian characteristics when $n = 1$ and $We = 0$. In the current work, the physical parameters of attention are the local skin friction coefficient $\left(C_{fx}\right)$ and the local Nusselt number $\left(Nu_x\right)$, which can be expressed as follows:

$$C_{fx} = \frac{\tau_w}{\rho_f \left(U_w\right)^2/2}, \quad Nu_x = \frac{q_w x}{k_f T_0}, \tag{20}$$

Here, the heat flux from the wall shear stress (τ_w) and the surface of the sheet (q_w) are given by Rehman *et al*. (2019)

$$\tau_w = \left\{ \mu_{hnf} \frac{\partial u}{\partial y} \left[1 + \lambda^2 \left(\frac{\partial u}{\partial y} \right)^2 \right]^{\frac{n-1}{2}} \right\}_{y=0}, \quad q_w = -k_{hnf} \left(\frac{\partial T}{\partial y} \right)\Big|_{y=0}. \tag{21}$$

Equantion (21) is obtained by using Eqs. (13)-(14) and inducing Eq. (22) into Eq. (21) as follows

$$\begin{aligned} &C_{fx} \operatorname{Re}_x^{1/2} = \frac{\mu_{hnf}}{\mu_f} 2 f''(0) \left\{ 1 + \frac{We^2}{R} \left[f''(0) \right]^2 \right\}^{\frac{n-1}{2}}, \\ &2 Nu_x \operatorname{Re}_x^{-3/2} \beta (1 - dt)^{1/2} \frac{k_f}{k_{hnf}} = \theta'(0). \end{aligned} \tag{22}$$

The local Reynolds number is defined as $\operatorname{Re}_x = \dfrac{x u_w(x,t)}{\nu_f}$.

3. Results and Discussion

This section aims to examine how crucial parameters affect the behavior of a stretched sheet in the Carreau fluid thin film boundary layer flow. Equations (15)-(16) were numerically resolved by the MATLAB program's bvp4c function, which solves boundary value problems (Shampine *et al*. 2003). Along with the boundary conditions given in Eq. (17) for the selected values of the hybrid nanoparticle volume fraction (ϕ_{hnf}), Weissenberg number (We), suction/injection parameter (S), unsteadiness parameter (σ), power-law index (n), and Prandtl number (Pr). The fixed ranges of the parameters' values are $(0.6 \le \sigma \le 1.2)$, $(-0.3 \le S \le 0.2)$, $(0 \le We \le 0.5)$ and $(0.6 \le n \le 1.6)$. Since the base fluid in the current study is CMC/water, the Prandtl number (Pr) is remained constant at 8 throughout the computation. The range of the hybrid nanoparticle volume fraction, ϕ_{hnf} is fixed at $\phi_{hnf} = \phi_1 + \phi_2 = 0.02 + 0.02 = 0.04$. The alumina nanoparticle volume fraction ϕ_1 is regarded as zero for the monotype nanofluid case. It is crucial to confirm the mathematical model as shown in Eqs. (15)-(17) and evaluate the effectiveness of the collocation method before discussing the current numerical results. The thin film flow problem examined by Wang (2006) has been analysed using the MATLAB program's bvp4c function. The outcomes are shown in Table 3 and Table 4 to evaluate the efficacy of the present method. The numerical findings and the prior analytical solutions agree very well.

Table 3: Numerical values comparison for $f''(0)$ when $m = Pr = 1$ and $We = M = S = 0$

S	R		$f''(0)$	
	Wang (2006)	Present output	Wang (2006)	Present output
0.6	3.13125	3.131710	−3.74233	−3.742786
0.7	2.57701	2.576995	−3.14965	−3.149614
0.8	2.15199	2151994	−2.68094	−2.680966
0.9	1.81599	1.815987	−2.29683	−2.296825
1.0	1.54362	1.543616	−1.97238	−1.972385

Table 4: $-\theta'(0)$ comparison value in Wang (2006) problem solution

S	$-\theta'(0)$	
	Wang (2006)	Present output
0.01	0.090474	0.090474
0.1	0.756162	0.756162
1	3.595970	3.595991
2	5.244150	5.259187
3	6.514440	6.533702

Figure 2(a) and Figure 2(b) reveal the impacts of various power-law index parameters n on the flow field for both hybrid nanofluid and mono nanofluid cases. As n rises from 0.6 to 1.6, the velocity profile diminishes. When the n value is increased, it means that the Carreau fluid signifies shear thickening $(n>1)$, yielding the fluid becoming more viscous for both hybrid and mono nanofluid cases. However, an increment in n contributes to the decrement of the fluid temperature, raising the heat flow and increasing the heat transfer rate over the sheet surface, as illustrated in Figure 2(b). These are the effects of a decreasing fluid viscosity on the current model.

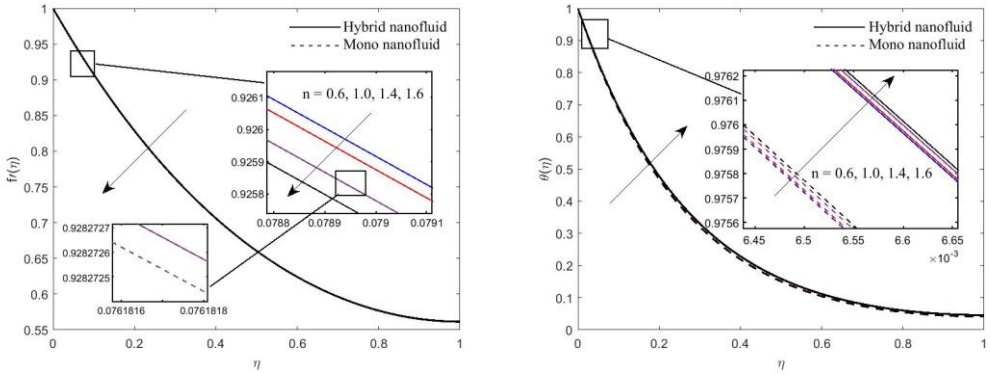

(a) (b)

Figure 2: Variation of n when $\sigma = 0.8$, $We = 0.2$, $S = -0.3$ and $Pr = 8$ for (a) velocity profiles, and (b) temperature profiles

Table 5 depicts the $C_{fx}\,\mathrm{Re}_x^{1/2}$ values as S varies for both hybrid nanofluid and mono nanofluid cases. The intensity of the injection increment when S decrementing from 0.2 to -0.3. As a consequence, the stretched sheet wall shear stress increases. The impacts on the velocity profiles of the various unsteadiness parameter for the injection case $(S<0)$ and suction case $(S>0)$, respectively, are depicted in Figure 3(a). It is noticed that the film thickness diminishes at the free surface when increasing injection and impacts a decline in fluid velocity. Even a permeable elastic sheet is stretched to induce fluid motion; altering the unsteadiness parameter value influences the velocity profiles. The thin film flow velocity is determined to drop for both cases of injection $(S<0)$ and suction $(S>0)$, when the unsteadiness parameter value is elevated. Hence, the injection case diminishes as the value S rises, and the suction case exhibits a similar trend in the temperature profiles, as shown in Figure 3(b). This occurs because of the unsteadiness parameter rising skin friction, which can lead to more heat being transmitted from the surface to the flow while raising the momentum of the fluid film. Thus, the thin fluid film of velocity and temperature consequently drops. Moreover,

when the wall is imposed with the injection effect $(S<0)$, the temperature of the thin liquid film increases. However, when the wall suction $(S>0)$ is applied, the fluid temperature decreases. The suction effect increases skin friction and reduces the liquid film temperature by inducing the boundary layer to adhere more firmly to the wall.

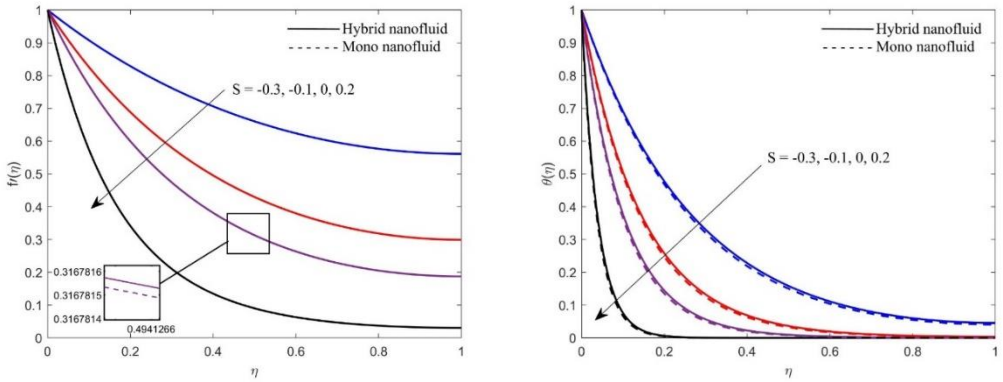

(a) (b)

Figure 3: Variation of S when $\sigma = 0.8,\ We = 0.2,\ n = 0.6$ and $Pr = 8$ for (a) velocity profiles, and (b) temperature profiles

Table 5: Numerical results of $C_{fx}\,\mathrm{Re}_x^{1/2}$ when $\sigma = 0.8,\ Pr = 8,\ We = 0.2$ and $n = 0.6$.

S	$C_{fx}\,\mathrm{Re}_x^{1/2}$	
	Hybrid Nanofluid $(\phi_1 = \phi_2 = 0.02)$	Mono Nanofluid $(\phi_1 = 0,\ \phi_2 = 0.02)$
-0.3	-2.2001099	-2.0895695
-0.1	-4.2927258	-4.0770440
0	-5.8482716	-5.5544317
0.2	-11.9442378	-11.3440953

Next, the difference between hybrid nanofluid and mono-typed nanofluid is minimal, as seen in Figure 4(a) and Figure 4(b). Furthermore, an increase in σ was observed to disperse heat and reduce the fluid temperature in the fluid regime. As a result, there is less heat flux at the accelerating sheet on the accelerated surface, where the heat transfer is diminished. When the fluid velocity increases through the permeable stretched sheet, the thickness of the film at the free surface decreases, enhancing the stretching sheet shear stress. Additionally, this phenomenon occurs. However, Figure 4(b) demonstrates the temperature profiles when the fluid temperature diminishes; the sheet surface of the heat flux and sigma value rises.

Typically, an increment We increases the fluid's relaxation time and eventually makes the fluid more resistant to flow. Figure 5(a) illuminates that the velocity profiles for the Carreau mono and hybrid nanofluids increase as the Weissenberg number rises. The Carreau fluid responds to external forces more gradually due to the increase in We, which explains a prolonged relaxation rate (Naganthran *et al*. 2021). Figure 5(b) depicts the temperature profiles in the region of the thin film. As We increases, the Carreau hybrid nanofluid, and mono nanofluid cases have a decrement in the temperature profile. As the fluid travels from the stretched sheet surface to the thin liquid layer, an increment in We enhances the fluid viscosity, resulting in flow retardation. Ultimately, the fluid temperature rises, increasing the stretching sheet's surface heat flux and accelerating the heat transfer rate.

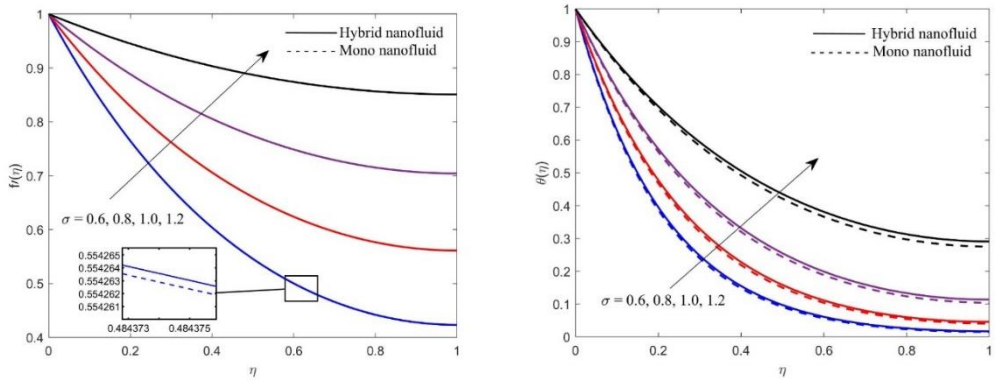

(a) (b)

Figure 4: Variation of σ when $We = 0,\ Pr = 8.2, S = -0.3$ and $n = 0.6$ for (a) velocity profiles, and (b) temperature profiles

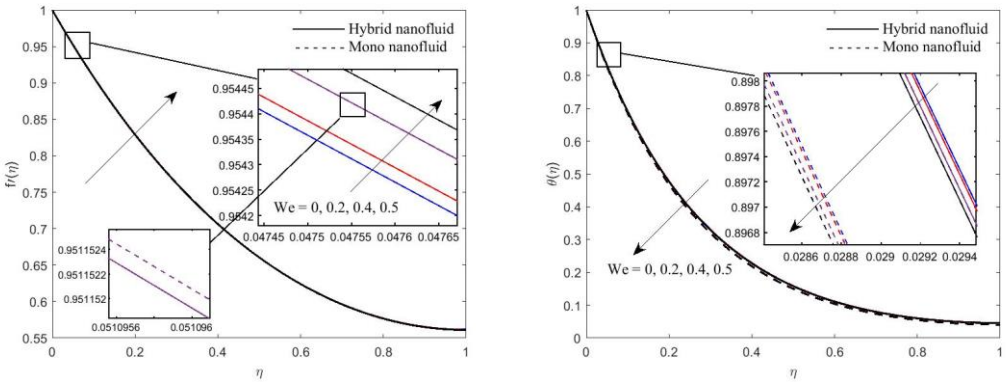

(a) (b)

Figure 5: Variation of We when $\sigma = 0.8,\ Pr = 8,\ S = -0.3$ and $n = 0.6$ for (a) velocity profiles, and (b) temperature profiles

4. Conclusion

The current work analysed the effects of suction/injection on the Carreau hybrid nanofilm in thin film flows through an unsteady stretched surface. In order to produce a hybrid nanofluid, the Al_2O_3 and Cu nanoparticles suspended in pure water have been evaluated. By adopting a similarity transformation, the governing partial differential equations are transformed into a system of ordinary differential equations, which are then computed employing the MATLAB (bvp4c) function. The impacts of hybrid nanoparticle volume fraction ϕ_{hnf}, Prandtl number Pr, injection/suction parameter S, Weissenberg number We, power-law index n, and unsteadiness parameter σ on the fluid flow were examined in this work. The findings of this study are that the suction parameters are more influencing the heat transfer rate and skin friction coefficient more than the injection parameters. The most significant impacts of the injection were discovered to be a decrement in film thickness and an improvement in convective heat transfer rates at the free surface. Hence, the fluid flow temperature rises for injection cases, whereas it falls for suction cases. Further, the thin film flow of velocity increases with the unsteadiness parameter in both injection and suction circumstances, reducing film thickness.

Acknowledgments

This work is funded by research grants from the Ministry of Higher Education Malaysia (FRGS/1/2020/STG06/UKM/01/1) and Universiti Kebangsaan Malaysia (TAP-K007136).

References

Abbasi F.M., Hayat T. & Alsaedi A. 2015. Numerical analysis for MHD peristaltic transport of Carreau-Yasuda fluid in a curved channel with Hall effects. *Journal of Magnetism and Magnetic Materials* **382**: 104–110.

Abo-Elkhair R.E., Bhatti M.M. & Mekheimer K.S. 2021. Magnetic force effects on peristaltic transport of hybrid bio-nanofluid (Au–Cu nanoparticles) with moderate Reynolds number: An expanding horizon. *International Communications in Heat and Mass Transfer* **123**: 105228.

Akbar N.S., Nadeem S., Haq R.U. & Ye S. 2014. MHD stagnation point flow of Carreau fluid toward a permeable shrinking sheet: Dual solutions. *Ain Shams Engineering Journal* **5**(4): 1233–1239.

Alabdulhadi S., Abu Bakar S., Ishak A., Waini I. & Ahmed S.E. 2023. Effect of buoyancy force on an unsteady thin film flow of Al_2O_3/water nanofluid over an inclined stretching sheet. *Mathematics* **11**(3): 739.

Ali R., Shahzad A., us Saher K., Elahi Z. & Abbas T. 2022. The thin film flow of Al_2O_3 nanofluid particle over an unsteady stretching surface. *Case Studies in Thermal Engineering* **29**: 101695.

Andersson H.I., Aarseth J.B. & Dandapat B.S. 2000. Heat transfer in a liquid film on an unsteady stretching surface. *International Journal of Heat and Mass Transfer* **43**(1): 69–74.

Bilal M., Saeed A., Gul T., Rehman M. & Khan A. 2021. Thin-film flow of Carreau fluid over a stretching surface including the couple stress and uniform magnetic field. *Partial Differential Equations in Applied Mathematics* **4**: 100162.

Boger D.V. 1977. Demonstration of upper and lower Newtonian fluid behaviour in a pseudoplastic fluid. *Nature* **265**: 126–128.

Carreau P.J. 1972. Rheological equations from molecular network theories. *Transactions of The Society Rheology* **16**: 99–127.

Choi S.U.S. & Eastman J.A. 1995. Enhancing thermal conductivity of fluids with nanoparticles. *ASME Fluids Engineering Division* **231**: 99–105.

Dandapat B.S., Santra B. & Andersson H.I. 2003. Thermocapillarity in a liquid film on an unsteady stretching surface. *International Journal of Heat and Mass Transfer* **46**(16): 3009–3015.

Iqbal K., Ahmed J., Khan M., Ahmad L. & Alghamd M. 2020. Magnetohydrodynamic thin film deposition of Carreau nanofluid over an unsteady stretching surface. *Applied Physics A: Materials Science and Processing* **126**(2): 1–13.

Khan N.S., Gul T., Kumam P., Shah Z., Islam S., Khan W., Zuhra S. & Sohail A. 2019. Influence of inclined magnetic field on Carreau nanoliquid thin film flow and heat transfer with graphene nanoparticles. *Energies* **12**(8): 1459.

Liu I.C. 2004. Flow and heat transfer of an electrically conducting fluid of second grade over a stretching sheet subject to a transverse magnetic field. *International Journal of Heat and Mass Transfer* **47**(19–20): 4427–4437.

Maity S., Ghatani Y. & Dandapat B.S. 2016. Thermocapillary flow of a thin nanoliquid film over an unsteady stretching sheet. *Journal of Heat Transfer* **138**(4): 1–8.

Minea A.A. 2017. Hybrid nanofluids based on Al_2O_3, TiO_2 and SiO_2: Numerical evaluation of different approaches. *International Journal of Heat and Mass Transfer* **104**: 852–860.

Mukhopadhyay S. 2013. Analysis of boundary layer flow over a porous nonlinearly stretching sheet with partial slip at the boundary. *Alexandria Engineering Journal* **52**(4): 563–569.

Myers T.G. 2005. Application of non-Newtonian models to thin film flow. *Physical Review E - Statistical, Nonlinear, and Soft Matter Physics* **72**(6): 1–11.

Naganthran K., Hashim I. & Nazar R. 2020a. Triple solutions of Carreau thin film flow with thermocapillarity and injection on an unsteady stretching sheet. *Energies* **13**(12): 3177.

Naganthran K., Hashim I. & Nazar R. 2020b. Non-uniqueness solutions for the thin Carreau film flow and heat transfer over an unsteady stretching sheet. *International Communications in Heat and Mass Transfer* **117**: 104776.

Naganthran K., Nazar R., Siri Z. & Hashim I. 2021. Entropy analysis and melting heat transfer in the Carreau thin hybrid nanofluid film flow. *Mathematics* **9**(23): 3092.

Narayana M. & Sibanda P. 2012. Laminar flow of a nanoliquid film over an unsteady stretching sheet. *International Journal of Heat and Mass Transfer* **55**(25–26): 7552–7560.

Oztop H.F. & Abu-Nada E. 2008. Numerical study of natural convection in partially heated rectangular enclosures filled with nanofluids. *International Journal of Heat and Fluid Flow* **29**(5): 1326–1336.

Rahman M.M. 2011. Locally similar solutions for hydromagnetic and thermal slip flow boundary layers over a flat plate with variable fluid properties and convective surface boundary condition. *Meccanica* **46**(5): 1127–1143.

Rehman S., Idrees M., Shah R.A. & Khan Z. 2019. Suction/injection effects on an unsteady MHD Casson thin film flow with slip and uniform thickness over a stretching sheet along variable flow properties. *Boundary Value Problems* **2019**(1): 1–24.

Shampine L.F., Gladwell I. & Thompson S. 2003. *Solving ODEs with MATLAB*. New York, USA: Cambridge University Press.

Sundar L.S., Singh M.K. & Sousa A.C.M. 2014. Enhanced heat transfer and friction factor of MWCNT-Fe_3O_4/water hybrid nanofluids. *International Communications in Heat and Mass Transfer* **52**: 73–83.

Suresh S., Venkitaraj K.P., Selvakumar P. & Chandrasekar M. 2011. Synthesis of Al_2O_3-Cu/water hybrid nanofluids using two step method and its thermo physical properties. *Colloids and Surfaces A: Physicochemical and Engineering Aspects* **388**(1–3): 41–48.

Takabi B. & Salehi S. 2014. Augmentation of the heat transfer performance of a sinusoidal corrugated enclosure by employing hybrid nanofluid. *Advances in Mechanical Engineering* **6**: 1–16.

Tham L.Y.S., Nazar R. & Pop I. 2012. Mixed convection flow at the lower stagnation point of a circular cylinder embedded in a porous medium filled by a nanofluid containing gyrotactic microorganisms. *Journal of Quality Measurement and Analysis (JQMA)* **8(**2): 45–63.

Tlili I., Samrat S.P., Sandeep N. & Nabwey H.A. 2021. Effect of nanoparticle shape on unsteady liquid film flow of MHD Oldroyd-B ferrofluid. *Ain Shams Engineering Journal* **12**(1): 935–941.

Tshehla M.S. 2011. The flow of a Carreau fluid down an incline with a free surface. *International Journal of Physical Sciences* **6**(16): 3998–4012.

Waini I., Ishak A. & Pop I. 2021a. Aliran titik genangan MHD dan pemindahan haba terhadap permukaan telap meregang/mengecut dalam nanobendalir hibrid. *Sains Malaysiana* **50**(9): 2819–2832.

Waini I., Ishak A. & Pop I. 2021b. Melting heat transfer of a hybrid nanofluid flow towards a stagnation point region with second-order slip. *Proceedings of the Institution of Mechanical Engineers, Part E: Journal of Process Mechanical Engineering* **235**(2): 405–415.

Wang C. 2006. Analytic solutions for a liquid film on an unsteady stretching surface. *Heat and Mass Transfer/Waerme- und Stoffuebertragung* **42**(8): 759–766.

Wang C.Y. 1990. Liquid film on an unsteady stretching surface. *Quarterly of Applied Mathematics* **48**(4): 601–610.

Xu H., Pop I. & You X.C. 2013. Flow and heat transfer in a nano-liquid film over an unsteady stretching surface. *International Journal of Heat and Mass Transfer* **60**(1): 646–652.

Zainal N.A., Nazar R., Naganthran K. & Pop I. 2020. Unsteady stagnation point flow of hybrid nanofluid past a convectively heated stretching/shrinking sheet with velocity slip. *Mathematics* **8**(10): 1649.

Zainal N.A., Nazar R., Naganthran K. & Pop I. 2021. MHD flow and heat transfer of hybrid nanofluid over a permeable moving surface in the presence of thermal radiation. *International Journal of Numerical Methods for Heat & Fluid Flow* **31**(3): 858–879.

Department of Mathematical Sciences
Faculty of Science and Technology
Universiti Kebangsaan Malaysia
43600 UKM Bangi
Selangor DE, MALAYSIA
E-mail: p109938@siswa.ukm.edu.my, rmn@ukm.edu.my, ishak_h@ukm.edu.my*

Institute of Mathematical Sciences
Center for Data Analytics Consultancy & Services
Faculty of Science
Universiti Malaya
50603 Kuala Lumpur, MALAYSIA
E-mail: kohi@um.edu.my

Received: 22 May 2023
Accepted: 21 August 2023

*Corresponding author